Abundant surface-semimetal phases in three-dimensional obstructed atomic insulators

Xianyong Ding [1,2,*] Xin Jin [3,4,*] Zhuo Chen,[1,2] Xuewei Lv,[4] Da-Shuai Ma [1,2,†] Xiaozhi Wu,[1,‡] and Rui Wang [1,2]

[1]*Institute for Structure and Function & Department of Physics, Chongqing University, Chongqing 400044, People's Republic of China*
[2]*Center of Quantum Materials and Devices, Chongqing University, Chongqing 400044, People's Republic of China*
[3]*College of Physics and Electronic Engineering, Chongqing Normal University, Chongqing 401331, China*
[4]*College of Materials Science and Engineering, Chongqing University, Chongqing 400044, China*

Three-dimensional obstructed atomic insulators (OAIs) are characterized by the appearance of floating surface states (FSSs) at specific surfaces. Benefiting from this feature, our study here shows the presence of abundant surface-semimetal phases in 3D OAIs. The symmetries of obstructed Wannier charge centers ensure the degeneracy of such FSSs at high-symmetry points or invariant lines in the surface Brillouin zone. Utilizing topological quantum chemistry theory, we identify a carbon allotrope with a body-centered tetragonal structure, named bct-C_{20}, as an ideal candidate for realizing different kinds of surface-semimetal phases. For the (001) surface of bct-C_{20}, there are four in-gap FSSs, and these four FSSs form two kinds of surface Dirac cones, i.e., topological Dirac cones with linear dispersion and symmetry-enforced quadratic Dirac cones. The band topology of a surface Dirac cone is captured by the effective surface Hamiltonian and the emergence of hinge states. Moreover, the existence of the surface-nodal-line state is also discussed. This work reports an approach to obtain d-dimensional semimetal phases from the surface states of $(d + 1)$-dimensional systems, which is of great significance for the studies in revealing topological states and their practical applications in high-dimensional crystals.

I. INTRODUCTION

Two-dimensional topological semimetal states enabled by crystalline symmetry are currently one of the most active research areas in condensed-matter physics [1–10]. Such semimetals are characterized by band topology protected band nodes with distinct energy dispersion, degree of degeneracy, and the dimension of the degeneracy manifold [11–15]. Systems with topologically nontrivial band nodes are proposed to possess many exotic physical properties such as ultrahigh carrier mobility [16–19], half-integer quantum Hall effects [20–23], large diamagnetism, and electromagnetic duality [24,25]. Thus, such systems are regarded as potential candidates for the next-generation quantum information technology revolution [1,26–29]. Nevertheless, the experimental research on two-dimensional (2D) topological states lags behind the theoretical one seriously [3,20–22,30–32]. The limited number of experimentally synthesized 2D topological materials, the non-negligible spin-orbit coupling, and the inevitable coupling to the substrate are the main reasons for this status quo. Therefore, achieving high-quality 2D topological semimetal states remains an ongoing question that needs to be addressed urgently.

Most recently, with the developing of topological quantum chemistry [33,34], symmetry indicator [35–38], real space invariant (RSI) [39,40], and related theories [41,42], the rapid developments in revealing the link between the emergence of quasiparticles and symmetry constraints are witnessed by both the physics and the materials science communities. These theories have undoubtedly made a major breakthrough in revealing the band degeneracy in the bulk states of 2D systems. In addition to the bulk state, we realize that it is feasible to realize d-dimensional semimetal states in the surface states of $(d + 1)$-dimensional obstructed atomic insulators (OAIs) [43,44] or unconventional materials [45]. In particular, the OAI is featured by the mismatch between Wannier charge centers and atom-occupied Wyckoff positions (WPs) [39,40,46]. Thus, this kind of nontrivial phase can be effectively diagnosed as an insulator whose band representations (BRs) can be expressed as a sum of elementary BRs with a *necessary* one induced by *orbitals* locating at the empty position W. W denotes the obstructed Wannier charge centers (OWCCs), which can be easily identified by RSI theory. Presently, various novel properties in OAIs have been proposed in both theoretical and experimental research, such as electrodes [47], catalysis [40], large shift current [48], superconductivity [49], and beyond [43–45,50–52]. Most importantly, with cleavage terminations cutting through OWCCs, floating surface states (FSSs) could appear within the bulk gap [43,45,50]. However, it is still unclear whether the 2D quasiparticles could emerge in the surface states of 3D OAIs and, if so, which system would be a candidate.

Here, we put forward a strategy to explore abundant 2D quasiparticles on surfaces of a 3D OAI. Due to the map from the 3D space group to the 2D layer group, we first elucidate

---

*These authors contributed equally to this work.
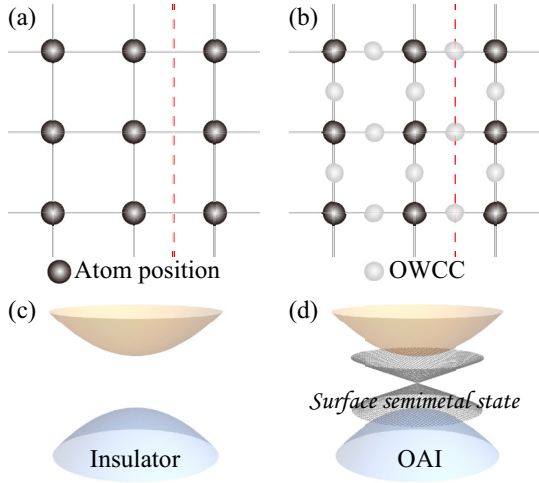†madason.xin@gmail.com
‡xiaozhiwu@cqu.edu.cn

FIG. 1. The sketch plot of an atomic insulator (a) and an OAI (b). The atom-occupied position and the OWCC are represented by the spheres in black and white, respectively. (c) There is no surface state in the bulk gap when the atomic insulator is cleaved. (d) When the OWCC is exposed on the surface, the 2D semimetal state emerges potentially. The cleavage terminations discussed in panels (c) and (d) are represented by the red dashed line in panels (a) and (b).

FIG. 2. Crystal structure of three-dimensional bct-C_{20}. (a) Bird's-eye and side views of the conventional unit cell for bct-C_{20} with a space group of $P4/mmm$ (No. 123). In this plot, different colors denote different Wyckoff positions. (b) The BZ and the corresponding (001) surface BZ of bct-C_{20}. (c) Energy versus volume of bct-C_{20} and other carbon analogs, i.e., cubic diamond, graphite, T-carbon [53], bct-C_{12} [54], bct-C_{16} [55], bct-C_{20}, bco-C_{16} [56], fco-C_6 [57], bct-C_{40} [58], oP-C_{24} [59], Pentagon Carbon [60], and Op16 [61] are also shown for comparison. (d) The phonon spectrum of bct-C_{20}.

that the 2D quasiparticles originate from a surface lattice formed by orbitals at OWCCs, whose symmetry guarantees that the FSSs degenerate at high-symmetry points or invariant lines in the surface Brillouin zone (BZ). We further show by first-principles calculations that a carbon allotrope, i.e., bct-C_{20}, can achieve our proposal. The energetic, mechanical, dynamical, and thermodynamic stability of bct-C_{20} are all verified. We reveal that the electronic band structure of bct-C_{20} has a wide band gap (> 1 eV), which was proved to belong to the OAI phase. Four in-gap FSSs appear at the (001) surface. One can simultaneously observe a topological Dirac cone with linear dispersion and a symmetry-enforced quadratic Dirac cone formed by these four FSSs. The symmetry protection mechanism of these surface Dirac cones is detailed discussed. The topology feature of the topological surface Dirac cone is depicted by the appearance of a hinge state and an effective surface Hamiltonian.

II. ARGUMENT TO REACH 2D TOPOLOGICAL SEMIMETAL PHASES

We start with an intuitive argument to elucidate the physical mechanism of how to reach the 2D semimetal phase in the surface states of 3D OAIs. Here, we ignored the spin-orbit couplings, a similar argument could be extended to the spinful case. As schematically shown in Figs. 1(a) and 1(b), in sharp contrast to atomic insulators, there are some orbitals pinned at the OWCCs in OAIs. When cleaved with these orbitals exposed on a specific surface, there would be FSSs as shown in Fig. 1(d). Physically, if the total number of orbitals exposed on the surface is odd, the emerging FSSs would be metallic, which is referred to as a filling anomaly [62]. As a comparison, when the number is even, each valence band is fully occupied. Then, there are two potential cases where we can find 2D quasi-particles: Case-I: two FSSs de-
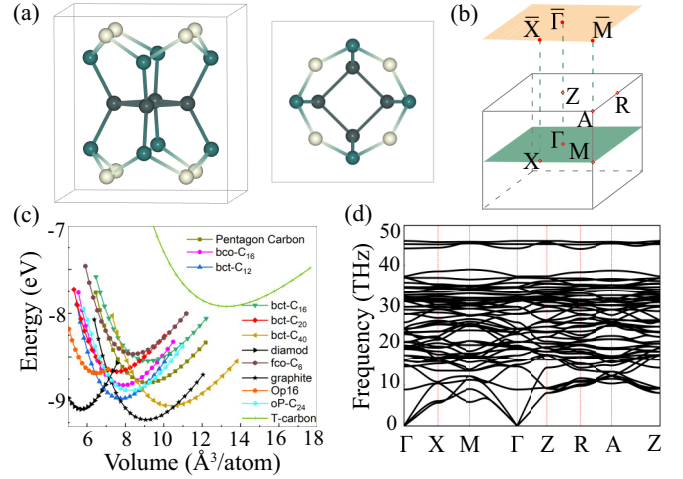
generate at the high-symmetry point $\overline{K}_s$ in the surface BZ and form a 2D irreducible representation of the little group at $\overline{K}_s$; Case-II: with the additional crystalline symmetry (e.g., mirror symmetry that is normal to the surface) that survived in the surface, there naturally would be symmetry (mirror)-protected 2D semimetal states when two FSSs with opposite symmetry eigenvalues cross on the symmetry (mirror)-invariant line in the surface BZ. The 2D nodal line state formed by surface states of OAIs and constrained by the nonsymmorphic symmetries is briefly discussed in Sec. V. In this work, both of the two cases are verified in bct-C_{20}.

III. THE STRUCTURE, STABILITY, AND ELECTRONIC PROPERTIES OF bct-C_{20}

The crystalline structure of bct-C_{20} is shown in Fig. 2(a). This system comprises 20 atoms arranged in a body-centered tetragonal structure with the space group $P4/mmm$ (No. 123). The optimized lattice constants are $a = b = 5.202$ Å and $c = 5.578$ Å. The carbon atoms in this system are distributed over three inequivalent WPs, i.e., $4o$ $(1/2, x, 1/2)$, $8t$ $(x, 1/2, z)$, and $8r$ (x, x, z). As shown in Fig. 2(a), the unit cell of bct-C_{20} is composed of four- and five-sided rings, and the adjacent cells are connected by hexagonal rings.

Here, we verify the energetic, mechanical, dynamical, and thermodynamic stability of bct-C_{20}. Comprehensive and detailed data supporting stability are available in the Supplemental Material (SM) [63]. As shown in Fig. 2(c), the total energies of different carbon analogs are obtained. The energy minimal -8.67 eV/atom of bct-C_{20} is less than that of T-carbon [53], bct-C_{16} [55], and fco-C_6 [57]. However, it is higher than that of graphite, diamond, bct-C_{40}, bct-C_{12},
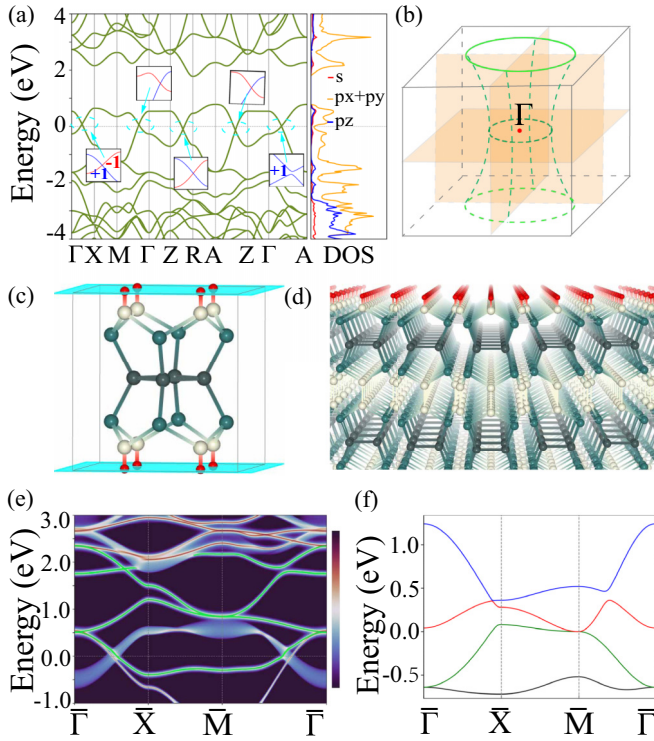
FIG. 3. (a) Projected band structure and density of states of bct-C_{20}, which is projected to s, $p_x + p_y$, and p_z orbitals. The insets are the symmetry eigenvalues for mirror symmetries $m_{x,y,z}$, in which the red line denotes the eigenvalue of -1 and the blue line denotes the eigenvalue of $+1$. Thus, the band crossings in the $k_{x,y,z} = 0, \pi$ plane are protected by mirror symmetries. (b) The schematic diagram of the nodal cage in the momentum space of bct-C_{20}. (c) The position of the obstructed Wannier charge center of bct-C_{20} is colored in red. (d) The semi-infinite (001) surface of bct-C_{20} with the OWCCs exposed on the surface. In this plot, only the OWCCs on the surface are shown. (e) Four FSSs are highlighted in blue within the energy windows $[-1\,\text{eV}, 2.5\,\text{eV}]$. (f) The band structure of the effective surface Hamiltonian. The four floating bands $FS_{k=1,2,3,4}$ are plotted in black, green, red, and blue, respectively.

oP-C_{24}, bco-C_{16}, and Pentagon Carbon [54,56,58–60]. The cohesive energy listed in Table S1 [63] also shows that bct-C_{20} has cohesive energy lower than that of some reported carbon analogs, e.g., T-carbon [53], bct-C_{16} [55], and fco-C_6 [57], which indicates the energetic stability of bct-C_{20}. To our best knowledge, the energy of T-carbon is highest among these carbon allotropes. Fortunately, it was synthesized in 2017 and 2020 [64,65]. Thus, it is promising to synthesize bct-C_{20} experimentally. The mechanical stability is confirmed by the independent elastic constants that satisfy the Born mechanical stability for the orthogonal crystal [63,66]. The dynamical stability of bct-C_{20} can be reflected by the phonon spectrum. As shown in Fig. 2(d), the phonon branches of bct-C_{20} have no imaginary frequency in the whole BZ. The Ab initio Molecular Dynamic (AIMD) simulations with a 10-ps timescale at $T = 300\,\text{K}$ demonstrate the thermodynamical stability of bct-C_{20}.

The calculated electronic bands of bct-C_{20} along the high-symmetry lines in BZ are shown in Fig. 3(a). The projected

bands and density of states predict that the states near the Fermi level are dominated by the E_u, i.e., $p_x + p_y$ orbitals of carbon atoms that occupy the Wyckoff position $8r\ (x, x, z)$ of bct-C_{20}, as shown in Fig. S2(a) of the SM [63]. Moreover, it is obvious that there are many band crossing points along the high symmetry lines, e.g., Γ-X, Γ-M, and Z-R. By carefully checking, we find that the band crossings in the whole BZ form a nodal cage, as shown in Fig. 3(b). We discuss the features in detail, e.g., the shape of the cage and the band topology of the nodal cage phase, in the SM [63]. Here, we show the projected local density of states for the (001) surface in Fig. 3(e). As shown in Fig. 3(e), there are many surface states with floating characteristics in the projected local density of states of the (001) surface, which we discuss in the next section.

IV. THE ABUNDANT SURFACE DIRAC CONES FOR THE OAI PHASE

Here, we prove that the FSSs on the (001) surface derive from the nontrivial topological phase, i.e., obstructed atomic insulator phase of the gap in the energy windows [1 eV, 2 eV]. The number of occupied bands, i.e., N_{Occ}, corresponding to the energy gap is 41. More importantly, for the first time, we show that the OAI phase provides an opportunity to achieve surface Dirac cones with different dispersion and band topologies. Specifically, in bct-C_{20}, we found that, due to the gap being in the OAI phase, there are two kinds of symmetry-restricted surface Dirac cones: topological Dirac cones with linear dispersion and symmetry-enforced quadratic Dirac cones.

To verify the band topology of the gap, here, we recall the definition of RSI [39,40,63]. Based on the band representation, RSI is defined at the specific Wyckoff position W. Nonzero RSI at W indicates that there are orbitals pinned at W. For the WP $4j$ whose site group is C_{2v}, highlighted by red balls in Fig. 3(d), the $\mathbb{Z}$ type RSI is written as

$$\delta(j) = \sum_{i=1,2} m(B_i) - m(A_i) = -2, \tag{1}$$

where the integer $m(\rho_{\omega_k})$ means the multiplicity of the irreducible representation ρ_{ω_k} that is defined at WP $4j$. The RSI $\delta(j) = -2$ implies that there are at least two orbitals, e.g., two s orbitals that are pinned at the unoccupied $4j$ Wyckoff position. Thus, the gap with $N_{\text{Occ}} = 41$ is in the OAI phase. As shown in Figs. 3(d) and 3(e), some FSSs occur when the OWCCs of the system are exposed on the (001) surface. It is worth noting that, the band connection of the FSSs is restricted by the symmetries that are maintained in the semi-infinite system with the open boundary condition applied for the [001] direction, as shown in Fig. 3(d). One observes in Fig. 3(e) that there are four visible floating surface bands within the energy windows $[-1\,\text{eV}, 2.5\,\text{eV}]$. These four bands are labeled as $FS_{k=1,2,3,4}$ ordered by energy at $\overline{X}$ and highlighted in different colors, i.e., black, green, red, and blue in Fig. 3(f). There are two kinds of band crossings formed by FSSs at $\overline{M}$, $\overline{\Gamma}$, and the high-symmetry line $\overline{\Delta}$, i.e., $\overline{\Gamma X}$. Here, we analyze the band dispersion and band topology of the two kinds of band crossings. The symmetries preserved in the semi-infinite system form a subgroup of $P4/mmm$, i.e., $P4mm$ (No. 99). And, the

OWCC is exactly at the $4d$ (x, x, z) WP of $P4mm$. Based on the nonzero RSI, we put s orbitals at the $4d$ WPs of $P4mm$ and construct an effective surface tight-binding Hamiltonian (see the derivation and the explicit expression of this Hamiltonian in the SM [63]). With appropriate couplings considered, as shown in Fig. 3(f) and the SM [63], the band structure of the effective surface Hamiltonian keeps in good agreement with that obtained by the Wannier function and shown in Fig. 3(e).

Here, we provide a comprehensive symmetry analysis and low-energy effective models to gain a thorough understanding of the presence of the doubly degenerated point located at $\overline{\text{M}}$. The generating elements of the space group $P4mm$ are fourfold rotation symmetry C_{4z}^+, mirror symmetry m_y, and time-reversal symmetry. Significantly, the little group at $\overline{\text{M}}$ has a 2D single-valued irreducible representation. By the calculation of the eigenvalues of symmetries, we get that the little group representation of the band crossing formed by FS_2 and FS_3 is M_5. Here, the band representation is written in the BCS convention [67]. Thus, this band degeneracy is symmetry enforced. To build an effective model, the basis state is chosen as $\psi = \{|m = 1\rangle, |m = -1\rangle\}$, with m being the eigenvalue of m_y. Under this basis, the matrix representations of m_y and $\mathcal{T}$ read

$$D(m_y) = \sigma_z, \quad D(\mathcal{T}) = -\sigma_0 \mathcal{K}, \qquad (2)$$

where σ_0 is the 2×2 identity matrix, σ_i ($i = x, y,$ and z) is the Pauli matrix, and $\mathcal{K}$ is the complex conjugate operator. Further, required by the following algebra

$$m_{x(y)}^2 = 1, \quad [m_x, m_y] = 0, \quad m_x m_y = (C_4^+)^2 = -1, \quad (3)$$

one can chose $D(C_{4z}^+) = i\sigma_y$. The effective Hamiltonian $H_{\overline{\text{M}}}(\boldsymbol{k})$ with this 2D band representation is required to satisfy $D(\mathcal{O})H_{\overline{\text{M}}}(\mathcal{O}^{-1}\boldsymbol{k})D^{-1}(\mathcal{O}) = H_{\overline{\text{M}}}(\boldsymbol{k})$. Hence, yielded by these symmetries, the explicit form of the minimal effective model is

$$H_{\overline{\text{M}}}(\boldsymbol{k}) = c_1(k_x^2 - k_y^2)\sigma_z + c_2 k_x k_y \sigma_x. \qquad (4)$$

The absence of the linear function of $k_{x,y}$ in Eq. (4) indicates that the dispersion of band crossing at $\overline{\text{M}}$ is quadratic. Similarly, for the band crossing formed by FS_1 and FS_2 at $\overline{\Gamma}$, since the little group representation is Γ_5, the crossing is also described by Eq. (4), which indicates the quadratic band dispersion and same symmetry protection mechanism as that at $\overline{\text{M}}$. When we turn to the band crossing on $\overline{\Delta}$ which is formed by FS_3 and FS_4, the obtained little group representations of FS_3 and FS_4 at an arbitrary k point are Δ_1 and Δ_2. Due to Δ_1 and Δ_2 carrying the opposite eigenvalues of mirror symmetry m_{100}, the band crossing on $\overline{\Delta}$ is mirror protected and exhibits linear dispersion, as schematically shown in Fig. 4(a). It is known that the mirror-protected linear band crossings in the 2D system possess nontrivial band topology. When clipped into a 1D nanoribbon, the characteristic edge state connecting projected points is in expectation, as schematically shown in Fig. 4(a). To verify this point, the energy spectrum of 1D bct-C$_{20}$ with the periodicity along the x direction maintained
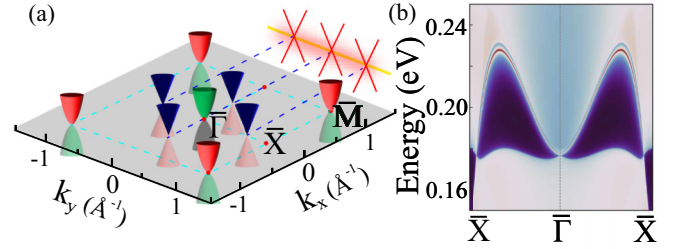

FIG. 4. (a) The schematic diagram of the abundant surface Dirac cones, i.e., quadratic Dirac cones at $\overline{\Gamma}$ and $\overline{\text{M}}$ and linear Dirac cones at $\overline{\Delta}$. The different colors of the Dirac cones represent different FSSs corresponding to those in Fig. 3(f). For a 1D nanoribbon, there will be hinge states (highlighted in orange) connecting the projects of linear surface Dirac cones (denoted by the red crosses). (b) The edge states of the effective surface Hamiltonian, which indicates the existence of the hinge state in bct-C$_{20}$.

is obtained and shown in Fig. 4(b). One observes that the emerging edge states indicate the system possesses metallic hinge states in bct-C$_{20}$.

V. DISCUSSION AND SUMMARY

In summary, we established a connection between the realization of 2D quasiparticles and the 3D OAI. The 2D topological states are protected by the symmetries maintained on the surface. Based on first-principles calculations, we realized our proposal in a funnel-like carbon phase bct-C$_{20}$, which possesses the structure, energetic, dynamic, and thermal stabilities. The calculated electronic structure and the symmetry analysis suggest that bct-C$_{20}$ possesses a nodal cage near the Fermi level. More importantly, we found a huge band gap with OAI band topology in the conduction band. When the OWCCs are exposed on the (001) surface, there will be four in-gap FSSs. The dispersion and band topology of the surface states are restricted by the symmetries maintained on the surface. Due to the large band gap, clean surface states and rich symmetries preserved on the surface of bct-C$_{20}$, abundant surface Dirac cones are allowed to be verified in bct-C$_{20}$, i.e., the symmetry-protected quadratic surface Dirac cones at $\overline{\Gamma}$ and $\overline{\text{M}}$ and topological linear surface Dirac cones on the high-symmetry line $\overline{\Delta}$. The band topology of the linear surface Dirac cone is verified by the hinge state. Furthermore, carbon is a light element and has negligible spin-orbital-coupling strength. Thus, these results shown in our manuscript can be extended to bosonic systems, which could be validated by optical or acoustic experiments.

We admit that the OAI gap in bct-C_{20} is in the conduction band, which would be an obstacle to the relevant experimental verification. Fortunately, the new progress obtained in the field of OAIs or unconventional materials makes the intrinsic OAI with 2D quasiparticles in FSSs accessible [43,45]. On the other hand, the emergence of the main interesting results of our work is beneficial from the featured FSSs. Naturally, the FSSs can form nodal line states. In the bulk states of a 2D or a 3D system, the nodal line could be protected by a combination of inversion and time-reversal symmetry $\mathcal{PT}$,

mirror symmetry $\mathcal{M}$, or nonsymmorphic symmetry $\hat{\mathcal{O}}$. As for the surface of a 3D system, both $\mathcal{P}$ and $\mathcal{M}$ parallel to the surface are destroyed. Hence, there would only be a $\hat{\mathcal{O}}$ protected nodal line on the surface of 3D OAIs. Our work would absolutely inspire interest in research concerning revealing the 2D topological states, e.g., the quantum spin Hall effect, the nodal line state, and topological flat bands in the FSSs of a higher-dimensional crystal.

[1] A. H. Castro Neto, F. Guinea, N. M. R. Peres, K. S. Novoselov, and A. K. Geim, Rev. Mod. Phys. **81**, 109 (2009).

[2] G. Palumbo and K. Meichanetzidis, Phys. Rev. B **92**, 235106 (2015).

[3] S. M. Young and C. L. Kane, Phys. Rev. Lett. **115**, 126803 (2015).

[4] Z. Wang, D.-K. Ki, H. Chen, H. Berger, A. H. MacDonald, and A. F. Morpurgo, Nat. Commun. **6**, 8339 (2015).

[5] B. Feng, B. Fu, S. Kasamatsu, S. Ito, P. Cheng, C.-C. Liu, Y. Feng, S. Wu, S. K. Mahatha, P. Sheverdyaeva *et al.*, Nat. Commun. **8**, 1007 (2017).

[6] L. Gao, J.-T. Sun, J.-C. Lu, H. Li, K. Qian, S. Zhang, Y.-Y. Zhang, T. Qian, H. Ding, X. Lin *et al.*, Adv. Mater. **30**, 1707055 (2018).

[7] S. Jeon, Y.-T. Oh, and Y. Kim, Phys. Rev. B **100**, 035406 (2019).

[8] B. Feng, R.-W. Zhang, Y. Feng, B. Fu, S. Wu, K. Miyamoto, S. He, L. Chen, K. Wu, K. Shimada *et al.*, Phys. Rev. Lett. **123**, 116401 (2019).

[9] C. Niu, J.-P. Hanke, P. M. Buhl, H. Zhang, L. Plucinski, D. Wortmann, S. Blügel, G. Bihlmayer, and Y. Mokrousov, Nat. Commun. **10**, 3179 (2019).

[10] Y. J. Jin, B. B. Zheng, X. L. Xiao, Z. J. Chen, Y. Xu, and H. Xu, Phys. Rev. Lett. **125**, 116402 (2020).

[11] X. Wan, A. M. Turner, A. Vishwanath, and S. Y. Savrasov, Phys. Rev. B **83**, 205101 (2011).

[12] C.-K. Chiu and A. P. Schnyder, Phys. Rev. B **90**, 205136 (2014).

[13] A. Bansil, H. Lin, and T. Das, Rev. Mod. Phys. **88**, 021004 (2016).

[14] A. Burkov, Nat. Mater. **15**, 1145 (2016).

[15] W. Luo, J. Ji, J. Lu, X. Zhang, and H. Xiang, Phys. Rev. B **101**, 195111 (2020).

[16] D. Xiao, M.-C. Chang, and Q. Niu, Rev. Mod. Phys. **82**, 1959 (2010).

[17] P. Hosur and X. Qi, C. R. Phys. **14**, 857 (2013).

[18] H. Wang, C.-K. Li, H. Liu, J. Yan, J. Wang, J. Liu, Z. Lin, Y. Li, Y. Wang, L. Li, D. Mandrus, X. C. Xie, J. Feng, and J. Wang, Phys. Rev. B **93**, 165127 (2016).

[19] J. Hu, S.-Y. Xu, N. Ni, and Z. Mao, Annu. Rev. Mater. Res. **49**, 207 (2019).

[20] K. S. Novoselov, A. K. Geim, S. V. Morozov, D. Jiang, M. I. Katsnelson, I. V. Grigorieva, S. Dubonos, and A. A. Firsov, Nature (London) **438**, 197 (2005).

[21] Y. Zhang, Y.-W. Tan, H. L. Stormer, and P. Kim, Nature (London) **438**, 201 (2005).

[22] K. S. Novoselov, Z. Jiang, Y. Zhang, S. Morozov, H. L. Stormer, U. Zeitler, J. Maan, G. Boebinger, P. Kim, and A. K. Geim, Science **315**, 1379 (2007).

[23] J.-Y. Zou, B. Fu, H.-W. Wang, Z.-A. Hu, and S.-Q. Shen, Phys. Rev. B **105**, L201106 (2022).

[24] S. Singh, N. Kumar, S. Roychowdhury, C. Shekhar, and C. Felser, J. Phys.: Condens. Matter **34**, 225802 (2022).

[25] S. Fujiyama, H. Maebashi, N. Tajima, T. Tsumuraya, H. B. Cui, M. Ogata, and R. Kato, Phys. Rev. Lett. **128**, 027201 (2022).

[26] M. N. Ali, J. Xiong, S. Flynn, J. Tao, Q. D. Gibson, L. M. Schoop, T. Liang, N. Haldolaarachchige, M. Hirschberger, N. P. Ong *et al.*, Nature (London) **514**, 205 (2014).

[27] J. Lai, X. Liu, J. Ma, Q. Wang, K. Zhang, X. Ren, Y. Liu, Q. Gu, X. Zhuo, W. Lu *et al.*, Adv. Mater. **30**, 1707152 (2018).

[28] Y. Wang, L. Wang, X. Liu, H. Wu, P. Wang, D. Yan, B. Cheng, Y. Shi, K. Watanabe, T. Taniguchi *et al.*, Nano Lett. **19**, 3969 (2019).

[29] D. Culcer, A. C. Keser, Y. Li, and G. Tkachov, 2D Mater. **7**, 022007 (2020).

[30] Y. Ren, Z. Qiao, and Q. Niu, Rep. Prog. Phys. **79**, 066501 (2016).

[31] D. Wang, F. Tang, J. Ji, W. Zhang, A. Vishwanath, H. C. Po, and X. Wan, Phys. Rev. B **100**, 195108 (2019).

[32] J. Ma, K. Deng, L. Zheng, S. Wu, Z. Liu, S. Zhou, and D. Sun, 2D Mater. **6**, 032001 (2019).

[33] B. Bradlyn, L. Elcoro, J. Cano, M. G. Vergniory, Z. Wang, C. Felser, M. I. Aroyo, and B. A. Bernevig, Nature (London) **547**, 298 (2017).

[34] L. Elcoro, B. J. Wieder, Z. Song, Y. Xu, B. Bradlyn, and B. A. Bernevig, Nat. Commun. **12**, 5965 (2021).

[35] H. C. Po, A. Vishwanath, and H. Watanabe, Nat. Commun. **8**, 1 (2017).

[36] J. Kruthoff, J. deBoer, J. vanWezel, C. L. Kane, and R.-J. Slager, Phys. Rev. X **7**, 041069 (2017).

[37] H. Watanabe, H. C. Po, and A. Vishwanath, Sci. Adv. **4**, eaat8685 (2018).

[38] Z. Song, T. Zhang, Z. Fang, and C. Fang, Nat. Commun. **9**, 1 (2018).

[39] Z.-D. Song, L. Elcoro, and B. A. Bernevig, Science **367**, 794 (2020).

[40] Y. Xu, L. Elcoro, G. Li, Z.-D. Song, N. Regnault, Q. Yang, Y. Sun, S. Parkin, C. Felser, and B. A. Bernevig, arXiv:2111.02433.

[41] B. Peng, Y. Jiang, Z. Fang, H. Weng, and C. Fang, Phys. Rev. B **105**, 235138 (2022).

[42] A. Bouhon, G. F. Lange, and R.-J. Slager, Phys. Rev. B **103**, 245127 (2021).

[43] X.-P. Li, D.-S. Ma, C.-C. Liu, Z.-M. Yu, and Y. Yao, Phys. Rev. B **105**, 165135 (2022).

[44] L. Wang, Y. Jiang, J. Liu, S. Zhang, J. Li, P. Liu, Y. Sun, H. Weng, and X.-Q. Chen, Phys. Rev. B **106**, 155144 (2022).

[45] J. Gao, Y. Qian, H. Jia, Z. Guo, Z. Fang, M. Liu, H. Weng, and Z. Wang, Sci. Bull. **67**, 598 (2022).

[46] Y. Xu, L. Elcoro, Z.-D. Song, M. Vergniory, C. Felser, S. S. Parkin, N. Regnault, J. L. Mañes, and B. A. Bernevig, arXiv:2106.10276.

[47] S. Nie, Y. Qian, J. Gao, Z. Fang, H. Weng, and Z. Wang, Phys. Rev. B **103**, 205133 (2021).

[48] R. Zhang, J. Deng, Y. Sun, Z. Fang, Z. Guo, and Z. Wang, Phys. Rev. Res. **5**, 023142 (2023).

[49] F. Schindler, B. Bradlyn, M. H. Fischer, and T. Neupert, Phys. Rev. Lett. **124**, 247001 (2020).

[50] Y. Aihara, M. Hirayama, and S. Murakami, Phys. Rev. Res. **2**, 033224 (2020).

[51] R. Banerjee, S. Mandal, and T. C. H. Liew, Phys. Rev. Lett. **124**, 063901 (2020).

[52] J. Kim, C.-Y. Huang, H. Lin, D. Vanderbilt, and N. Kioussis, Phys. Rev. B **107**, 045135 (2023).

[53] X. L. Sheng, Q. B. Yan, F. Ye, Q. R. Zheng, and G. Su, Phys. Rev. Lett. **106**, 155703 (2011).

[54] X. Dong, M. Hu, J. He, Y. Tian, and H.-T. Wang, Sci. Rep. **5**, 1 (2015).

[55] X.-Y. Ding, C. Zhang, L.-Y. Gan, Y. Cao, L.-L. Chen, and R. Wang, New J. Phys. **22**, 073036 (2020).

[56] J.-T. Wang, H. Weng, S. Nie, Z. Fang, Y. Kawazoe, and C. Chen, Phys. Rev. Lett. **116**, 195501 (2016).

[57] C. Zhang, X.-Y. Ding, L.-Y. Gan, Y. Cao, B.-S. Li, X. Wu, and R. Wang, Phys. Rev. B **101**, 235119 (2020).

[58] J.-T. Wang, S. Nie, H. Weng, Y. Kawazoe, and C. Chen, Phys. Rev. Lett. **120**, 026402 (2018).

[59] K. Bu, Y. Qian, J.-T. Wang, and H. Weng, Phys. Rev. B **103**, L081108 (2021).

[60] C. Zhong, Y. Chen, Z.-M. Yu, Y. Xie, H. Wang, S. A. Yang, and S. Zhang, Nat. Commun. **8**, 1 (2017).

[61] K. Bu, J.-T. Wang, H. Weng, and C. Chen, Phys. Rev. B **101**, 205104 (2020).

[62] W. A. Benalcazar, T. Li, and T. L. Hughes, Phys. Rev. B **99**, 245151 (2019).

[63] See Supplemental Material at http://link.aps.org/supplemental/10.1103/PhysRevB.108.085135 for details of the calculations, the additional discussion of the stability of bct-C_{20}, the topological nodal cage in the bulk state, and the effective surface model Hamiltonian, which include Refs. [39,40,52,66,68–81].

[64] J. Zhang, R. Wang, X. Zhu, A. Pan, C. Han, X. Li, D. Zhao, C. Ma, W. Wang, H. Su *et al.*, Nat. Commun. **8**, 683 (2017).

[65] K. Xu, H. Liu, Y.-C. Shi, J.-Y. You, X.-Y. Ma, H.-J. Cui, Q.-B. Yan, G.-C. Chen, and G. Su, Carbon **157**, 270 (2020).

[66] F. Mouhat and F. X. Coudert, Phys. Rev. B **90**, 224104 (2014).

[67] G.-B. Liu, M. Chu, Z. Zhang, Z.-M. Yu, and Y. Yao, Comput. Phys. Commun. **265**, 107993 (2021).

[68] G. Kresse and J. Furthmüller, Phys. Rev. B **54**, 11169 (1996).

[69] P. Hohenberg and W. Kohn, Phys. Rev. **136**, B864 (1964).

[70] W. Kohn and L. J. Sham, Phys. Rev. **140**, A1133 (1965).

[71] J. P. Perdew, K. Burke, and M. Ernzerhof, Phys. Rev. Lett. **77**, 3865 (1996).

[72] H. J. Monkhorst and J. D. Pack, Phys. Rev. B **13**, 5188 (1976).

[73] J. Heyd, G. E. Scuseria, and M. Ernzerhof, J. Chem. Phys. **118**, 8207 (2003).

[74] S. Baroni, S. de Gironcoli, A. Dal Corso, and P. Giannozzi, Rev. Mod. Phys. **73**, 515 (2001).

[75] A. Togo and I. Tanaka, Scr. Mater. **108**, 1 (2015).

[76] N. Marzari, A. A. Mostofi, J. R. Yates, I. Souza, and D. Vanderbilt, Rev. Mod. Phys. **84**, 1419 (2012).

[77] A. A. Mostofi, J. R. Yates, Y.-S. Lee, I. Souza, D. Vanderbilt, and N. Marzari, Comput. Phys. Commun. **178**, 685 (2008).

[78] J. Gao, Q. Wu, C. Persson, and Z. Wang, Comput. Phys. Commun. **261**, 107760 (2021).

[79] F. Occelli, P. Loubeyre, and R. LeToullec, Nat. Mater. **2**, 151 (2003).

[80] R. Hill, Proc. Phys. Soc., London, Sec. A **65**, 349 (1952).

[81] D.-S. Ma, J. Zhou, B. Fu, Z.-M. Yu, C.-C. Liu, and Y. Yao, Phys. Rev. B **98**, 201104(R) (2018).